Numerical simulations of impacts during Surface Mechanical Attrition Treatment using crystal plasticity model with finite element method

Zhenglin Chen, Zhidan Sun, Delphine Retraint, Benoît Panicaud*

Université de Technologie de Troyes (UTT) – CNRS, Institut Charles Delaunay (ICD) /LASMIS, 12 rue Marie Curie, 10004 Troyes, France
*corresponding author: benoit.panicaud@utt.fr

Abstract:

Surface Mechanical Attrition Treatment (SMAT) is able to transform the top surface layer of materials from coarse grains to nano-sized grains by severe plastic deformation. SMAT is based on multidirectional mechanical impacts between balls and the surface of material. In this work, a crystal plasticity model introduced in finite element analysis, which takes into account the microstructure, is used to investigate the plastic activities due to the impacts between balls and the surface of material. A phenomenological crystal plasticity model implemented through user-defined ABAQUS subroutines is used in this work to perform numerical simulations. A set of parameters are studied such as ball size, crystal orientation, impact velocity, incident angle. The influences of these different parameters on plastic slip activities are analyzed. The first results demonstrate the interests of such numerical simulations for this specific process.

Keywords: SMAT, Surface nanocrystallization, Crystal plasticity, Finite element method, Impact simulation

1 Introduction

Surface Mechanical Attrition Treatment (SMAT) is a promising mechanical surface modification technique, which is able to transform the surface layer of coarse-grained materials to ultra-fine sized grains by means of severe plastic deformation [1, 2]. The nanocrystallization is due to the consequence of multi-directional impacts between the balls and the surface of material at high strain rate (Fig. 1). Indeed, as the strain rate is high and the cumulative plastic strain is large in the region close to the surface, a great number of crystallographic defects such as plastic slips and deformation twins can be generated at the top surface, which progressively leads to the formation of a nanostructured layer. Simultaneously, high compressive residual stresses may be introduced in the SMAT affected region. Thanks to the nanostructured layer and the compressive residuals stresses, SMAT allows to significantly improve the mechanical properties of materials [2, 3].

Due to excellent mechanical properties of SMATed materials, it is necessary and useful to investigate the SMAT process both experimentally and numerically in order to obtain a better understanding and better controlling of the process. Experimental studies, extensively performed previously in the literature [4], have shown that the mechanical properties of SMATed materials are highly influenced by the microstructure such as grain size and by the mechanical state such as work hardening. From a modeling perspective, it would be highly beneficial to establish accurate numerical models of SMAT process in order to consider the influence of the different parameters at different scales.
In order to study the basic plastic slip activities generated during SMAT, in this work, a crystal plasticity model was used to study the deformation process of monocrystal due to the impacts of balls. Finite element simulations were performed to analyze the effects of different parameters including ball diameter, crystal orientation, ball velocity and incident impact angle.

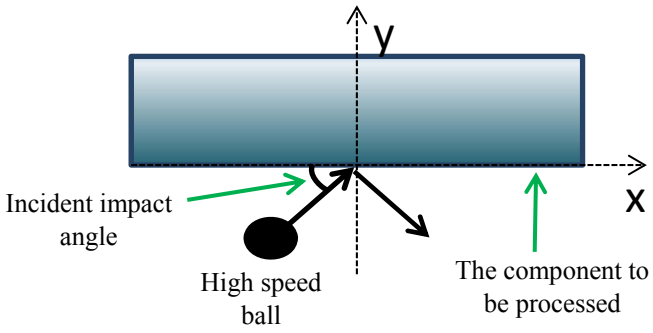

Fig. 1. Schematic description of the SMAT process.

2 Kinematics and constitutive law of crystal plasticity

The kinematics used in the field of crystal plasticity conforms to the classical multiplicative decomposition of the deformation gradient after Lee et al. [5]. The deformation gradient F is assumed to be a decomposition of elastic and inelastic parts:

$$F = F_e F_p \tag{1}$$

where elastic part F_e corresponds to pure elastic deformation (stretching) and possible rigid body rotation. The inelastic part F_p is assumed to be solely related to the slip deformation. Accordingly, the velocity gradient can be calculated by:

$$L = \dot{F}F^{-1} = L_e + L_p \tag{2}$$

The velocity gradient in the current configuration is given by [6]:

$$L_p = \sum_{s=1}^{N} \dot{\gamma}^s \left(\underline{\mathbf{l}}^s \otimes \underline{\mathbf{n}}^s \right) \tag{3}$$

where $\dot{\gamma}^s$ is the plastic slip rate on the slip system. The evolution of the plastic deformation can be expressed as follows [6]:

$$\dot{F}_p = L_p F_p \tag{4}$$

In this work, to model the behavior of a copper alloy, a time-dependent kinetic formulation developed by Méric and Cailletaud [7] was used. The Méric-Cailletaud model transposes the isotropic and kinematic hardening models used in the macroscopic scale to the scale of slip system. This model takes into account the strain hardening on slip systems, especially through the components of a work

hardening interaction matrix. It connects the isotropic work hardening due to different slip systems, and thus takes into account the effects of latent hardening. The crystallographic slip rate $\dot{\gamma}^s$ on the slip system *s* is expressed as a power law function of the resolved shear stress τ^s :

$$\dot{\gamma}^s = \left\langle \frac{\left|\tau^s - \chi^s\right| - \kappa^s}{g} \right\rangle^n \operatorname{sgn}\left(\tau^s - \chi^s\right) \tag{5}$$

where g and n are viscosity parameters; n determines the material rate dependence; χ^s is the kinematic hardening variable; κ^s is the isotropic strain hardening variable. The kinematic hardening variable χ^s is associated with the kinematic state variable α^s which is a vector with a length equal to the number of slip systems. The kinematic hardening can be written through a nonlinear evolution of χ^s :

$$\chi^s = C\alpha^s \quad \text{with} \quad \dot{\alpha}^s = \dot{\gamma}^s - D\left|\dot{\gamma}^s\right|\alpha^s \tag{6}$$

where *C* and *D* are material constants.

The isotropic strain hardening variable κ^s is expressed as follows:

$$\kappa^s = \kappa_0 + Q\sum_{r=1}^{N} h^{sr}\left(1 - \exp\left(-B\upsilon^r\right)\right) \quad \text{with} \quad \dot{\upsilon}^r = \left|\dot{\gamma}^r\right| \tag{7}$$

where κ_0 is the initial critical resolved shear stress, and h^{sr} is the interaction matrix between slip systems accounting for self (r=s) and latent (r≠s) hardening. Note that in this work $h^{sr} = 1$ was taken, which corresponds to the case of Taylor hardening. The nonlinear hardening is described by an exponential function with two phenomenological constants *Q* and *B*. *Q* characterizes the hardening capability and *B* is a coefficient characterizing the saturation rate of isotropic hardening. $q^s = 1 - \exp\left(-B\upsilon^r\right)$ is the dual thermodynamic variable of κ^s , and its evolution law is given as:

$$\dot{q}^s = B\left(1 - q^s\right)\left|\dot{\gamma}^s\right| \tag{8}$$

which represents the evolution of the dislocation density.

By integrating the slip rate $\dot{\upsilon}^r$ (always positive), the cumulative plastic slip can be calculated. This cumulative plastic slip of one slip system is quantified independently of the slip direction (which can change during the deformation) as follows:

$$\upsilon^r(t) = \int_0^t \left|\dot{\gamma}^r\right| dt \tag{9}$$

A fully anisotropic elasticity tensor is considered for modeling the elastic response of the crystal with elastic constants expressed using Voigt notation:

$$C_0 = \begin{bmatrix} C_{11} & C_{12} & C_{12} & 0 & 0 & 0 \\ & C_{11} & C_{12} & 0 & 0 & 0 \\ & & C_{11} & 0 & 0 & 0 \\ & & & C_{44} & 0 & 0 \\ & sym & & & C_{44} & 0 \\ & & & & & C_{44} \end{bmatrix} \tag{10}$$

where C_{11} , C_{12} and C_{44} are material constants. Thus, for Hookean materials, the expression of the Cauchy's stress tensor is as follows:

$$\sigma = C_e : \varepsilon_e \tag{11}$$

where C_e is the fourth rank tensor of elastic moduli, for which the case of a cubic lattice rotated by a rotation matrix R with respect to the global coordinate system takes the following form:

$$C_e = R^T \cdot R^T \cdot C_0 \cdot R \cdot R \tag{12}$$

3 Finite element model

A three-dimensional finite element model was built using the commercial finite element (FE) code ABAQUS 6.13 to investigate plastic slips induced during SMAT process by single impact. As shown in Fig. 2, the FE model consists of a rigid ball impacting the center of a surface of the monocrystal with dimensions of $5 \times 5 \times 2.5 \ mm^3$. The bottom of the monocrystal model was fully constraint, i.e. no displacement and rotations are possible. The friction between the ball and the surface of the monocrystal is Hard contact in normal contact direction and the friction coefficient is 0.3 in the tangential contact direction. To ensure the calculation accuracy, the mesh size in the region close to the impact contact point is much finer than other areas. The type of mesh was set as C3D8I: an 8-node linear brick element with incompatible modes.

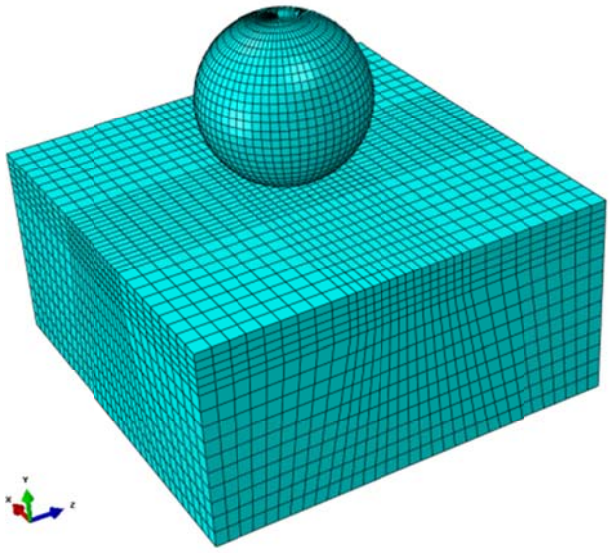

Fig. 2. FE model describing single impact on a surface of a monocrystal by a rigid ball.

4 Results and discussion

It is not easy to numerically model the SMAT process, since the SMAT is a process involving lots of random balls impacts against the surface of material [8]. In this work, we only consider that the center region of the monocrystal is impacted by a ball. We aim to investigate the effects of various parameters such as ball diameter, crystal orientation, ball velocity and incident angle on the cumulative plastic strain in order to better understand the SMAT process.

4.1 Influence of ball diameter

Fig. 3 shows the distribution of cumulative plastic strain obtained by numerical simulations with different ball diameters. Two ball diameters were used and they are respectively d = 2 mm and d = 3 mm. The crystallographic orientation of the monocrystal with respect to the vertical impact direction (incident angle = 90°) is [001], and the velocity of ball is v = 6 m/s. According to Fig. 3, the equivalent plastic strain is much higher for the case of 3 mm ball, compared to the one of 2 mm ball. The maximum plastic strain is increased from 0.0004 to 0.0019 when the diameter changes from 2 mm to 3 mm. Another phenomenon which can be observed is related to the fact that the width of curve on the abscissa is larger for the case of 3 mm ball. This means that the size of plastic deformation zone is larger when the ball size is increased. The increase of plastic slip activities due to larger ball is linked to higher kinetic energy of the ball. As a matter of fact, the kinetic energy is cube of the ball diameter [9], and thus the kinetic energy of the 3 mm ball is higher than the 2 mm ball. During the impact between the ball and the material, a certain quantity of kinetic energy of the flying ball was transformed into potential energy stored in the material in the form of plastic deformation. In the case of 3 mm ball, the energy stored in the material should be much higher compared to the case of 2 mm ball.

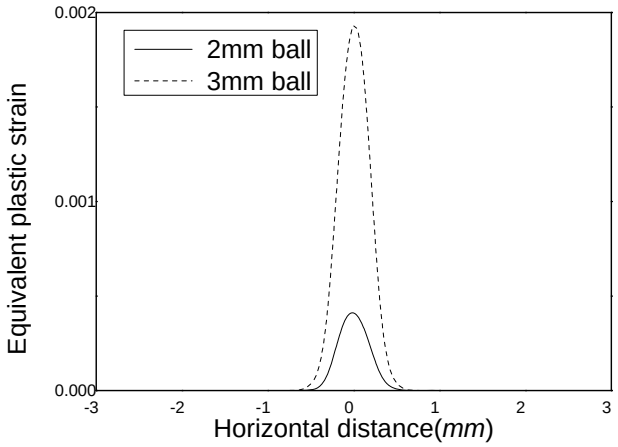

Fig. 3. Plastic strain distribution obtained with impacts using different ball diameters.

4.2 Influence of crystal orientation

In order to investigate the influence of crystal orientation on plastic slip activities due to impact loading, three crystallographic orientations were used. These orientations respectively correspond to [001], [011] and [111] with respect to the vertical impact direction. To realize these simulations, the following conditions are used: ball diameter d = 2 mm, ball velocity v = 10 m/s and impact angle θ = 90°. Fig. 4 presents the results of the plastic strain distribution as function of horizontal distance from one border of the model. It can be seen that the plastic strain was considerably influenced by crystal orientation. The obtained plastic strain with [111] is much higher than those of the other two orientations, which means that in the case of [111], it is easier to activate plastic slips, compared to the [001] and [011] orientations. This result seems not consistent with the single crystal plasticity theory for face centered cubic (FCC) materials. In a FCC crystal, when a uniaxial load is applied following the orientation [111], there are six non-zero Schmid factors equal to 0.27, whereas in the

orientation [001], there are eight non-zero Schmid factors equal to 0.41[10]. This means that in [111] directions, the activation of plastic slips is more difficult, and consequently the plastic strain level should be lower. This discrepancy between the simulation result and the crystal plasticity theory could be due to the fact that even under unidirectional impact loading, the stress state is much complex according to the Hertzian contact theory [11]. The stress state beneath the contact area is of three-dimensional nature, and other slip systems should have been activated in the case of [111] orientation. Further analysis on plastic slip activation of each slip system will be systematically performed.

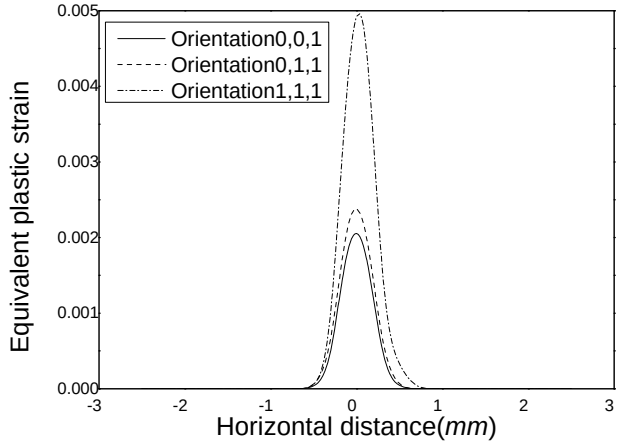

Fig. 4. Distribution of plastic strain with different crystal orientations of [001], [011] and [111] with respect to the vertical impact direction.

4.3 Influence of ball velocity

The influence of the ball velocity was investigated with ball velocities equal to v = 6 m/s, 8 m/s and 10 m/s, respectively. In the SMAT process, the ball velocity can be changed by varying the output power of the ultrasonic generator. For these simulations, the crystal orientation is [001], and the impact angle is $\theta = 90°$ (vertical impact). Fig. 5 shows the distribution of plastic strain obtained with different ball velocities. It can be seen that the level of plastic strain is increased with the increase of ball velocity. The effect of ball velocity is also related to the kinetic energy, which is similar to the case of ball size, as presented in Section 4.1. There is an energy transformation from the kinetic form to the potential form, and the energy is stored in the material for example as plastic deformation energy. Higher ball velocity gives higher kinetic energy of balls, which can induce higher energy transformation during the impact with the material. It is important to note that the influence of ball velocity is particularly important for a highly strain-rate dependent material. Furthermore, the strain rate in the material induced by ball impact is increased with the increase of ball velocity, which can promote the formation of strain-induced twins. However, in this study of the strain-induced twinning is not taken into account.

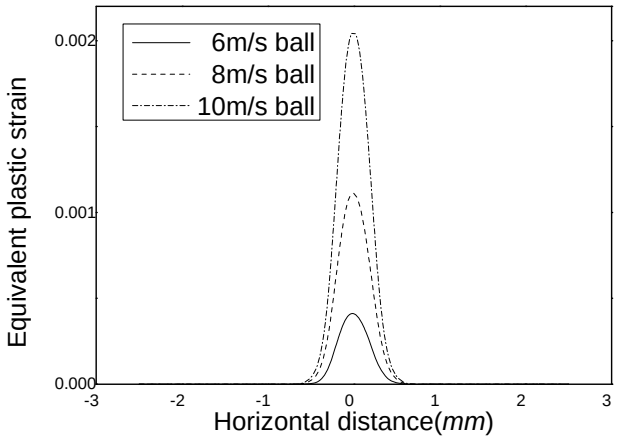

Fig. 5. Plastic strain distribution obtained with different ball velocities.

4.4 Influence of impact angle

The influence of incident impact angle was also studied. The incident impact angle corresponds to the angle with respect to the surface of the material, as schematically presented in Fig. 1. In this work, three angles chosen are respectively 60°, 75° and 90°. The crystal orientation of the material is [001]. The ball velocity is v = 10 m/s and the ball diameter is d = 2 mm. The result showing plastic strain is presented in Fig. 6. It can be seen that the level of plastic strain is highest for 90°, i.e. vertical impact to the surface, and the values decrease with the decrease of the incident angle. This phenomenon is consistent with the fact that the component of the ball velocity vector normal to the surface $v_y = v\sin\theta$ is decreased with the decrease of the incident angle. Thus the effective ball velocity is actually lower when the angle is decreased.

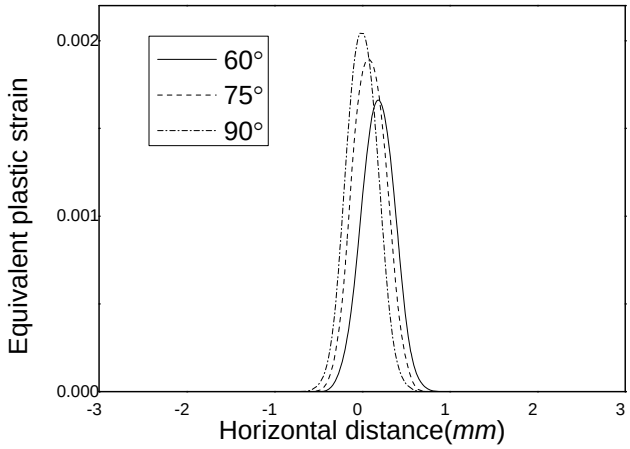

Fig. 6. Plastic strain induced by impacts following different impact angles.

5 Conclusions

Impact simulations using crystal plasticity finite element method were carried out in this work in order to study the effect of different parameters involved in SMAT process including ball size, crystal orientation, ball velocity and incident impact angle. The first results show that larger ball size, higher ball velocity and larger incident impact angle lead to higher plastic strain, which is consistent with the kinetic energy theory. While changing the crystal orientation, the activation of plastic slips seem become more complex due to the three-dimensional nature of the stress state beneath the impact surface according to the Hertzian contact theory. These first results demonstrate that the crystal plasticity finite element method is an interesting tool to understand the mechanisms of material transformation during SMAT process. Future work aims to systematically study the plastic slip activities on each slip system induced by ball impacts for both monocrystal and polycrystal.

References

[1] K. Lu, J. Lu, Nanostructured surface layer on metallic materials induced by surface mechanical attrition treatment, Materials Science and Engineering A 375 (2004) 38-45.
[2] T. Roland, D. Retraint, K. Lu, J. Lu, Fatigue life improvement through surface nanostructuring of stainless steel by means of surface mechanical attrition treatment, Scripta Materialia 54 (2006) 1949-1954.
[3] T. Roland, D. Retraint, K. Lu, J. Lu, Enhanced mechanical behavior of a nanocrystallised stainless steel and its thermal stability, Materials Science and Engineering A 445 (2007) 281-288.
[4] Y. Liu, B. Jin, J. Lu, Mechanical properties and thermal stability of nanocrystallized pure aluminum produced by surface mechanical attrition treatment, Materials Science & Engineering A 636 (2015) 446-451.
[5] E.H. Lee, D.T. Liu, Finite‐Strain Elastic - Plastic Theory with Application to Plane‐Wave Analysis, Journal of Applied Physics 38 (1967) 19-27.
[6] J.R. Rice, Inelastic constitutive relations for solids: An internal-variable theory and its application to metal plasticity, Journal of the Mechanics and Physics of Solids 19 (1971) 433-455.
[7] L. Méric, G. Cailletaud, M. Gaspérini, FE calculations of copper bicrystal specimens submitted to tension-compression tests, Acta Metallurgica et Materialia 42 (1994) 921-935.
[8] X.C. Zhang, J. Lu, S.Q. Shi, A Computational Study of Plastic Deformation in AISI 304 Induced by Surface Mechanical Attrition Treatment, Mechanics of Advanced Materials & Structures 18 (2011) 572-577.
[9] W.Y. Tsai, J.C. Huang, Y.J. Gao, Y.L. Chung, Relationship between microstructure and properties for ultrasonic surface mechanical attrition treatment, Scripta Materialia 103 (2015) 45-48.
[10] B. Clausen, T. Lorentzen, T. Leffers, Self-consistent modelling of the plastic deformation of f.c.c. polycrystals and its implications for diffraction measurements of internal stresses, Acta Materialia 46 (1998) 3087-3098.
[11] T. Brittain, Shear stresses below asperities in Hertzian contact as measured by photoelasticity, Journal of Lubrication Technology Transactions of the ASME 95 (1973) 277-286.